Cement and Concrete Research 40 (2010) 1041–1051

Contents lists available at ScienceDirect

Cement and Concrete Research

journal homepage: http://ees.elsevier.com/CEMCON/default.asp

Relating rapid chloride transport parameters of concretes to microstructural features extracted from electrical impedance

Narayanan Neithalath [a,*], Jitendra Jain [a,b]

[a] Department of Civil and Environmental Engineering, Clarkson University, Potsdam, NY 13699, United States
[b] School of Civil Engineering, Purdue University, West Lafayette, IN, United States

ARTICLE INFO

Article history:
Received 14 April 2009
Accepted 28 February 2010

Keywords:
Transport properties (C)
Electrical properties (C)
Electrical impedance spectroscopy
Porosity
Pore connectivity factor

ABSTRACT

The rapid chloride transport parameters such as the rapid chloride permeability (RCP) and non-steady state migration coefficient are related to the material microstructural parameters in this paper. Electrical impedance spectroscopy and associated equivalent circuit modeling are used to extract the microstructural features of the plain concrete as well as concretes modified with varying amounts of Class F fly ash or silica fume. A methodology is developed in this paper that utilizes the ratios of RCP values and the ratios of effective conductivities to pore solution conductivities of plain and modified concretes, to quantify the relative influence of pore solution conductivity and pore structure on the RCP values. The resistance attributable to the connected pores is extracted from an equivalent circuit model for the impedance spectra of concretes, which is found to relate well to the rapid chloride transport parameters as well as the microstructural parameters. Based on the experimental results and electrical circuit models, it is shown that a reduction in pore connectivity has a higher impact on the rapid chloride transport parameters than a reduction in the porosity, and reduction in pore sizes is more consequential than porosity reduction in reducing pore connectivity.

1. Introduction

Chloride induced corrosion of reinforcing steel is one of the major deterioration mechanisms in reinforced concrete that has been receiving significant attention worldwide because of its widespread occurrence and the costs associated with repairing and maintaining damaged structures. A number of mechanisms are responsible for the transport of chloride ions in concrete including absorption due to capillary action, diffusion (movement of the ions under a concentration gradient, or strictly under a chemical potential), migration in an electric field, or permeation driven by pressure gradients. However, it is accepted that diffusion is the primary means by which chlorides are transported to the level of reinforcing steel in saturated concretes in the absence of an electric field [1].

Chloride transport through concrete is influenced by the pore structure and the interaction between the ions and the pore walls [2]. The results of any chloride transport test method usually provide a value that is representative of the combination of both these effects. The pore structure depends on the water-to-cement ratio, the presence of supplementary cementing materials, and the age of the concrete. The influence of supplementary cementing materials in densifying the pore structure and affecting the mobility of chloride ions has been well documented [3–5]. The interaction between the chloride ions and the pore walls could be chemical (chloride binding predominantly by the aluminate phases [6–8]) or physical (surface forces binding the chlorides to pore walls).

The measurement of chloride transport parameters has been a topic of much interest, with a variety of methods being used in practice. ASTM has standardized three test methods: (i) C 1202, rapid chloride penetration test (RCPT), (ii) C 1443, 90 day ponding test, and (iii) C 1556, bulk diffusion test based on NT Build 443. RCPT is one of the most commonly employed chloride transport test methods because of its ease of use, even though there are serious limitations to this test, which are well recorded [9–11]. Other commonly used rapid tests that provide an indication of the chloride transport resistance of concretes are an electrical migration based test (NT Build 492[12]), and a steady state chloride conduction test [13]. The transport parameters determined from different test methods cannot be directly compared [14,15] even though indirect relationships might exist between some of them. An example is the relationship between the non-steady state migration coefficient from NT Build 492 test method and the diffusion coefficient from the ASTM C 1443 salt ponding test [16].

Electrical impedance spectroscopy (EIS), which is a powerful method to characterize the microstructure of cement based materials [17–19], has also been used to evaluate the chloride diffusivity in concrete [20,21]. A few studies [22,23] have used electrical impedance to monitor the microstructural changes that occur during and after

* Corresponding author. Tel.: +1 315 268 1261; fax: +1 315 268 7985.
E-mail address: nneithal@clarkson.edu (N. Neithalath).

0008-8846/$ – see front matter © 2010 Elsevier Ltd. All rights reserved.
doi:10.1016/j.cemconres.2010.02.016

chloride penetration. This paper uses EIS on concrete specimens before and after the rapid chloride transport tests to extract the pertinent features of the microstructure that are relevant to chloride transport.

The major objectives of this work are threefold: (i) to relate the effective electrical conductivity determined using EIS before the chloride ingress to the rapid chloride transport parameters of plain and fly ash or silica fume modified concretes, (ii) to quantify the relative influence of pore solution conductivity and pore structure refinement on the measured RCP values of fly ash and silica fume modified concretes, and (iii) to establish pore size–porosity–pore connectivity relationships and understand the relative influence of these pore structure features on rapid chloride transport parameters.

2. Experimental program

2.1. Materials and mixtures

A Type I Ordinary portland cement conforming to ASTM C 150, a Class F fly ash (FA) conforming to ASTM C 618, and a dry densified silica fume (SF) were used as the cementing materials in this study. The physical and chemical characteristics of these materials are shown in Table 1. Concrete mixtures having a water-to-cementing materials ratio (w/cm) of 0.40 were proportioned using natural sand and 12.5 mm nominal maximum size coarse aggregates. In addition to a control concrete, two mixtures were made with each of the cement replacement materials — either 10% or 20% of cement being replaced by fly ash, or 6% or 9% replaced by silica fume, by mass. The cementitious materials content was maintained at 430 kg/m^3 for all the mixtures. The high range water reducing admixture dosage was adjusted to produce slumps of 150 ± 15 mm. After mixing, the concrete was cast in 100 mm$\times$200 mm cylindrical molds and cured for either 28, 56, or 90 days in a moist environment before they were prepared for the chloride transport tests or porosity determination.

2.2. Test methods

Three different test methods were employed to evaluate chloride transport in the concrete mixtures. In addition, electrical impedance spectroscopy (EIS) measurements were carried out on concrete specimens. Porosity of concrete specimens was also determined using a vacuum saturation method at chosen ages of curing. The following sub-sections explain all the tests used.

2.2.1. Chloride transport test methods

Rapid chloride permeability test (RCPT), as per ASTM C 1202 was carried out on 50 mm thick discs cut from 200 mm long cylindrical specimens after 28, 56, and 90 days of moist curing. The specimens were vacuum saturated in water before subjecting them to the RCP test. This test provides an indication of the penetrability of chloride ions through concrete under a potential difference of 60 V. Though this test has been shown to have numerous disadvantages, it is still being widely used as a quality control measure, primarily because of its ease of use.

Table 1
Chemical composition and physical properties of the binders used in this study.

Composition (% by mass)/property	Cement	Silica fume	Fly ash
Silica (SiO_2)	20.2	93.4	50.24
Alumina (Al_2O_3)	4.7	0.42	28.78
Iron oxide (Fe_2O_3)	3.0	0.52	5.72
Calcium oxide (CaO)	61.9	1.91	5.86
Magnesium oxide (MgO)	2.6	–	1.74
Sodium oxide (Na_2O)	0.19	0.25	0.20
Potassium oxide (K_2O)	0.82	0.79	0.84
Sulfur trioxide (SO_3)	3.9	0.34	0.51
Loss on ignition	1.9	2.3	2.8
Median particle size (μm)	13	<1[a]	20
Density (kg/m^3)	3150	2200	2400

[a] Agglomerates can be even coarser than the cement particles.

Non-steady state migration (NSSM) test was carried out on 50 mm thick concrete discs after the respective curing durations, in accordance with NT Build 492 [12]. The specimens were preconditioned by vacuum saturating with calcium hydroxide solution. The catholyte and anolyte solutions used were 2 N NaCl and 0.3 N NaOH respectively. An initial voltage of 30 V was applied, and initial current recorded. The applied voltage and test duration were chosen based on the initial current. For all the specimens tested in this study, the applied voltage was between 30 V and 60 V. For the silica fume modified concretes, the denser matrix necessitated a higher voltage because of the lower initial currents. The test duration was maintained at 24 h for all the cases. After the test duration, the specimens were axially split and sprayed with a 0.1 M silver nitrate solution, and the depth of chloride penetration was measured based on the precipitation of white silver chloride. The non-steady state migration coefficient (D_{nssm}) in m^2/s is given as:

$$D_{nssm} = \frac{RT}{zFE}\frac{x_d - \alpha\sqrt{x_d}}{t} \tag{1}$$

$$\alpha = 2\sqrt{\frac{RT}{zFE}}\, erf^{-1}\left(1-\frac{2c_d}{c_0}\right) \tag{2}$$

where $E=(U-2)/L$, U is the absolute voltage (V), L is the specimen thickness in m, z is the valence of the chloride ion, F is the Faraday constant, R is the molar gas constant, T is the average value of initial and final temperatures in K, x_d is the average value of the penetration depth in m, t is the test duration in s, c_d is the chloride concentration at which silver nitrate changes to silver chloride (0.07 N), and c_0 is the chloride concentration of the catholyte solution (2 N).

Steady state chloride conduction tests (SSC) were also carried out on 25 mm thick concrete disc specimens based on the procedure described in [13]. The specimens were oven dried at 50 °C prior to the test to ensure complete saturation with a 5 M NaCl solution under vacuum. A voltage of 10 V was applied between a steel cathode and a graphite anode immersed in 5 M NaCl, and the potential across the specimen was measured using copper–copper sulfate half cells. The steady state conductivity (σ_{SSC}) was calculated based on the current (i), sample thickness (L), cross-sectional area (A), and the potential difference (V) as:

$$\sigma_{SSC} = \frac{iL}{VA} \tag{3}$$

2.2.2. Electrical impedance spectroscopy

Electrical impedance spectroscopy (EIS) was employed on specimens similar to that used for the RCP test. The RCP cell with the 50 mm thick specimens and the anolyte and catholyte (0.3 N NaOH and 3% NaCl) in place was used. EIS measurements were conducted in this study using a Solartron 1260™ impedance/gain-phase analyzer that was interfaced with a personal computer for data acquisition. The frequency of the EIS measurements ranged from 10 Hz to 1 MHz using a 250 mV AC signal, with 10 measurements per decade. The effective specimen conductivity (σ_{eff}) was determined from the bulk resistance (R_b) obtained from EIS (abscissa of the intersection of the bulk and electrode arcs in a Nyquist plot) as:

$$\sigma_{eff} = \frac{L}{R_b A} \tag{4}$$

where L and A are the specimen length and cross-sectional area respectively.

In the RCP cell, there is typically a gap of about 2–3 mm between the electrode mesh and the specimen, which is filled with the anolyte or the catholyte. From the conductivities of 3% NaCl and 0.3 N NaOH (4.4 and 5.7 S/m respectively), and the geometry of the RCP cell, the resistances of the solutions in these gaps were calculated to be less than 1 Ω, which can be neglected when compared to the R_b values of concrete which are 500 to 1000 times higher. Similar observations are reported in [24] also.

2.2.3. Measurement of concrete porosities

The porosities of hardened concretes were determined using a vacuum saturation method described in RILEM CPC 11.3 [25]. 50 mm thick discs were cut from 100 mm × 200 mm concrete cylinders, and oven dried at 100 °C for 24 h to remove all the evaporable water. The masses of the specimens were measured after allowing them to return to room temperature. The specimens were then subjected to vacuum saturation for 3 h, water was then allowed into the vacuum chamber while vacuum was maintained, and the vacuuming continued for an additional 1 h. The specimens were then left undisturbed in water for 12 more hours. The masses of the specimens were then recorded. The difference in the masses, converted into volume, represents the volume of capillary pores. Two specimens were used for each mixture at each age, and the average values of porosities were used for the analysis.

3. Rapid chloride transport and conductivity

3.1. RCP values and non-steady state migration coefficients

Fig. 1(a) shows the results of the RCP test on the plain and modified concretes after 28, 56, and 90 days of curing. The influence of silica fume in reducing the RCP values is immediately evident from this figure, whereas fly ash at early ages show RCP values similar to that of the plain concrete. However, the influence of pozzolanic reaction of fly ash is evident at later ages. Concretes with higher silica fume content show lower RCP values, as expected. Since the use of silica fume as a cement replacement material is known to reduce the pore solution conductivity [26] in addition to densifying the microstructure, the observed reduction in RCP values can be assumed to be a result of the combination of both the effects. In a later section of this paper, quantification of the relative effects of the reduction in pore solution conductivity and microstructure densification on the observed RCP values is detailed. The non-steady state migration coefficients (D_{nssm}) for the plain and modified concretes at all ages determined using Eqs. (1) and (2) are shown in Fig. 1(b). The influence of silica fume in significantly reducing the migration coefficients at all ages, and that of fly ash in moderately reducing the D_{nssm} values at later ages are evident from this figure.

3.2. Relating conductivities to RCP and D_{nssm} values

The relationship between the initial conductivities of concretes (just before the RCP or NSSM tests were started) determined using EIS from Eq. (4), and the RCP and D_{nssm} values are presented in Fig. 2(a) and (b) respectively. From Fig. 2(a), it is clearly seen that the initial conductivities before the start of the RCP test and the RCP values are linearly correlated with a very high coefficient of correlation. This is an indication that RCP is essentially a conductivity (or resistivity) test, as mentioned by several authors [9,27]. The relationship between the initial conductivities and the D_{nssm} values is shown in Fig. 2(b). The correlation, though good, is weaker than that between the conductivities and RCP values. The specimens that deviate conspicuously from linearity (i.e. lower D_{nssm} for the same initial conductivity) are the fly ash modified mixtures. One probable reason for this observation could be the increased amounts of aluminates in fly ash modified mixtures that result in some amount of chloride binding. The higher chloride concentration in the catholyte solution (2 M) during the NSSM test has been shown to result in the formation of some amounts of Friedel's salt in fly ash modified mixtures [28].

The steady state conductivity (σ_{SSC}) test is easier to perform, making it a viable alternative to the RCP test to study chloride transport. Since the specimens were saturated with a chloride solution of high concentration (5 M NaCl), the effects of pore solution conductivity are minimized when different specimens are compared. However, the exposure to a chloride solution of very high concentration might potentially result in the formation of chloride binding products even before the start of the test and thus alter the microstructure. Fig. 3(a) depicts the relationship between σ_{SSC} and the initial conductivity from EIS before the RCP test (σ_{EIS}), which shows a linear trend. The σ_{SSC} values are almost a magnitude higher than σ_{EIS} because of the conductivity of the 5 M NaCl solution (experimentally determined as 31 S/m) used to saturate the SSC test specimens. Using the values of σ_{SSC}, the steady state diffusion coefficient (D_{SSC}) can be calculated using Nernst–Einstein equation as:

$$\frac{\sigma_{SSC}}{\sigma_0} = \frac{D_{SSC}}{D_0} \tag{5}$$

where σ_0 is the conductivity of the 5 M NaCl solution used to saturate the specimen before the SSC test (31 S/m), and D_0 is the diffusivity of chloride ions in pore solution. The value of D_0 is taken as 1.1×10^{-9} m^2/s, by extrapolation from the data provided in [29] (where D_0 values

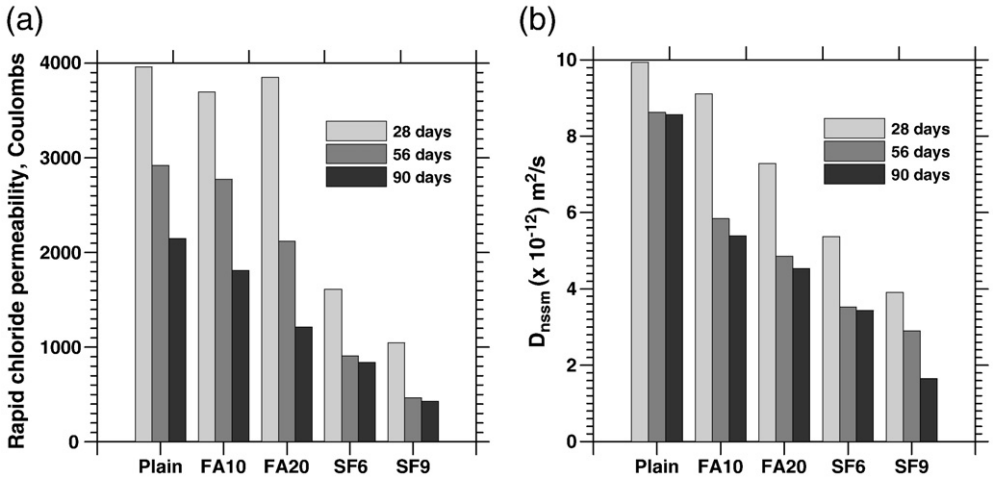

Fig. 1. (a) Rapid chloride permeability, and (b) non-steady state migration coefficients for plain and modified concretes.

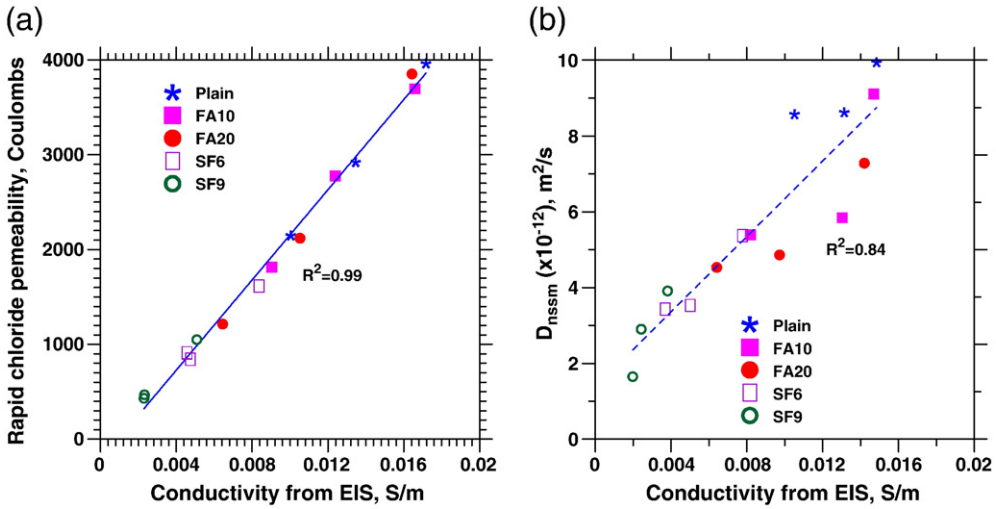

Fig. 2. Relationship between concrete conductivities from EIS and: (a) Rapid chloride permeability values, and (b) Non-steady state migration coefficients.

for Cl^- in NaCl solutions of 0.1 M to 4 M are given, which follows a linear trend). Fig. 3(b) shows the steady state diffusivities plotted against the non-steady state migration coefficients. In general, D_{nssm} is found to be higher than D_{SSC}, in line with the results reported in [30].

4. Quantification of the dependence of RCP values on pore solution conductivity and pore structure

It is well known that in the RCP test, the pore solution conductivity influences the measured results. Silica fume modified concrete mixtures typically contain pore solution of much lower conductivity than that of plain concrete because of the strong absorption of the alkali ions by the pozzolanic hydration products. Thus it would be incorrect to assume that silica fume modified concretes are "*x*" times better than plain concrete in reducing chloride permeability, where "*x*" is the ratio of the RCP values of plain concrete to those of the silica fume modified concretes. This section looks at the relative influence of the pore solution conductivity (σ_{pore}) and pore structure on the RCP values. Since the RCP test is effectively a conductivity test, a modified parallel model for effective conductivity (σ_{eff}) is used, which can be expressed as:

$$\sigma_{eff} = \sigma_{pore}(\phi\beta) \quad (6)$$

where ($\phi\beta$) is a lumped pore structure parameter, which is the product of porosity (ϕ) and pore connectivity factor (β). This expression assumes that the material under consideration is a porous medium with a single conducting phase (the pore phase). Though ϕ and β have been determined separately later in this paper, the lumped term $\phi\beta$ is used in this section in order to represent the features of the pore phase in a single term.

The pore solution conductivities (σ_{pore}) of the plain and modified concretes were obtained from the equivalent ionic conductivities of the highly conductive species in the pore solution (OH^-, Na^+, and K^+), the ionic concentrations, and the species valences [31]. The ionic concentration was obtained from the cement and the replacement materials content, w/c (or w/p), and the degrees of hydration of cement pastes. A methodology to predict the alkali ion concentrations in pore solutions has been detailed in [32]. Data on degrees of hydration of cement pastes containing the chosen dosages of fly ash or silica fume are reported in [33,34]. Limited validation on the use of this method to determine the conductivity of simulated pore solutions is reported in [31]. A recent study [35] has shown that there is good agreement between the early age values of the measured (from extracted pore solutions) and predicted pore solution conductivities of cement pastes made using different w/c. Fig. 4 shows the σ_{pore} values of the plain and modified pastes from 14 days until 90 days of curing. The plain and fly ash modified concretes have similar σ_{pore} values at all ages, whereas the

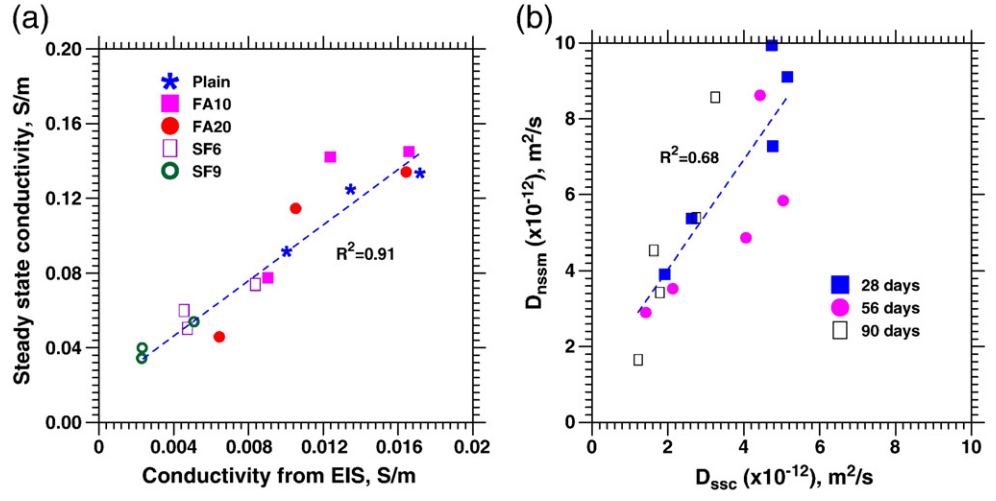

Fig. 3. Relationship between: (a) conductivities from EIS and the steady state conductivities, and (b) steady state diffusion coefficients and non-steady state migration coefficients.

silica fume modified concretes have lower σ_{pore} values than the other mixtures. Increase in cement replacement level by silica fume results in decrease in σ_{pore}.

Based on the measured effective conductivities and predicted pore solution conductivities, two conductivity ratios are defined as follows:

$$\sigma^*_{eff} = \frac{(\sigma_{eff})_{modified-concrete}}{(\sigma_{eff})_{plain-concrete}} \quad (7a)$$

$$\sigma^*_{pore} = \frac{\left(\sigma_{pore}\right)_{modified-concrete}}{\left(\sigma_{pore}\right)_{plain-concrete}}. \quad (7b)$$

The parameters of these equations are self explanatory. Using Eq. (6) for σ_{eff} in Eq. (7a), and dividing Eq. (7b) by Eq. (7a) gives

$$\frac{\sigma^*_{pore}}{\sigma^*_{eff}} = \frac{(\phi\beta)_{plain-concrete}}{(\phi\beta)_{modified-concrete}} = (\phi\beta)^*. \quad (8)$$

Table 2 shows the $(\phi\beta)^*$ values before and after the RCP test for all the mixtures studied, at 28 and 90 days of curing. The $(\phi\beta)^*$ values before the test were obtained by using the effective conductivities (σ_{eff}) and the pore solution conductivities (σ_{pore}) of specimens before they were subjected to chloride ion ingress. In order to determine the $(\phi\beta)^*$ values after the RCP test, the effective conductivities of all the specimens were measured after the end of the 6 h duration of the RCP test. The ohmic heating during the RCP test causes an increase in the pore solution conductivity. It has been stated that for every 1 °C increase in temperature due to the RCP test, a 2% increase in σ_{pore} can be reasonably assumed [36]. The pore solution conductivities shown in Fig. 4 were modified based on the recorded increase in temperature, and the $(\phi\beta)^*$ values after the RCP test determined. The temperature increase ranged from 10 °C to 15 °C for the plain concrete, 6 °C to 12 °C for the fly ash modified concretes, and 3 °C to 6 °C for the silica fume modified concretes.

If the pore structure of the plain and modified concretes are very similar (i.e., if $\phi\beta$ for the plain and modified mixtures are close to each other), then the ratio as determined from Eq. (8) should be equal to or very close to 1.0. As can be seen from Table 2, this indeed is the case for fly ash modified concretes at early ages, where microstructural changes would not have occurred yet because of the delayed pozzolanic reaction. A higher value of $(\phi\beta)^*$, which implies a lower value of $\phi\beta$ for the modified concretes, whether before or after the RCP test, implies better refinement of the pore structure. For the fly ash modified concretes at later ages, and silica fume modified concretes at all ages, the values of $(\phi\beta)^*$ before the test are greater than 1.0, indicating pore structure refinement as compared to the control concrete. When the $(\phi\beta)^*$ values before and after the RCP test are compared, it can be seen that there is a reduction in $(\phi\beta)^*$ values after the test, indicating that the material microstructure is being changed as a result of the RCP test. Hence the forthcoming discussion is centered on $(\phi\beta)^*$ before the test because it reflects the state of the pore structure unaltered by the conditions of the RCP test.

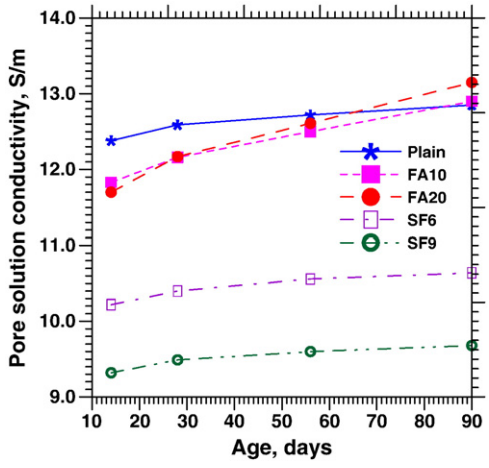

Fig. 4. Change in pore solution conductivity for the plain and modified concretes as a function of time.

Table 2 also shows the ratios of RCP values (RCP value of the plain concrete divided by that of the modified mixture — denoted as "x" at the start of this section). The ratio of RCP values for the fly ash modified concretes is also close to 1.0 at early ages, similar to the values of $(\phi\beta)^*$. At later ages for fly ash modified concretes, and at all ages for silica fume modified concretes, the "x" values are greater than $(\phi\beta)^*$. While the "x" values denote the combined influence of pore solution conductivity and pore structure (including the effects of temperature rise as a result of RCP test) on the measured RCP values, the $\sigma^*_{pore}/\sigma^*_{eff}$ or $(\phi\beta)^*$ values shown in Table 2 reflect the influence of pore structure refinement on RCP values, compared to those of plain concretes.

If the values of both the ratios shown in Table 2 (x and $(\phi\beta)^*$ before the test) for a particular mixture at a certain age are close to each other, it shows that the reduction in RCP values as compared to the plain concrete is attributable almost entirely to the pore structure changes. This is the case for fly ash modified concretes. For the silica fume modified concretes, the ratios of RCP values (x) are greater than $(\phi\beta)^*$. This shows that the reduction in RCP values of these mixtures as compared to the plain concrete is due to a combination of reduced pore solution conductivity as well as a refined pore structure. When $(\phi\beta)^*$ (before the test) is divided by the ratio of RCP values, the silica fume modified mixtures show values between 0.66 and 0.75 while fly ash modified concretes show values above 0.90. This means that 66–75% of the reduction in RCP values of the chosen silica fume modified mixtures, and more than 90% for the fly ash modified mixtures as compared to the plain concrete (depending on the curing duration and the replacement material content) can be attributed to pore structure refinement brought about by the incorporation of these replacement materials. The methodology described here provides an easy and concise means to quantify the relative effects of pore solution conductivity and pore structure refinement on the change in RCP values as a result of the use of cement replacement materials. The only measurement needed in addition to the charge passed from RCPT is the conductivity of the specimens before the RCP test is started, which can be easily obtained from the initial current (at time zero) when the RCP test is started. The pore solution conductivity can be obtained using the methodology described in [31], which is provided in an easy-to-use web interface [36]. If the temperature increase from RCP test is also recorded, an indication of the change in pore structure due to the test ($(\phi\beta)^*$ after the test) can also be obtained.

5. Porosity–pore connectivity–pore size relationships and their relative influence on chloride transport parameters

5.1. Porosity, pore connectivity and their relationships

The porosities (ϕ) of the plain and modified concretes at all ages, as determined by the vacuum saturation procedure described earlier, are shown in Table 3. Using the values of σ_{eff} and σ_{pore} as obtained in the previous section along with the values of ϕ, the values of pore connectivity (β) were extracted for all the mixtures at all ages using Eq. (6), and are plotted in Fig. 5. The plain concrete expectedly has the highest β values at all ages, followed by the fly ash modified mixtures, with the silica fume modified mixtures showing the least β values. A linear trend is observed between β and both RCP and D_{nssm} values as can be observed in Fig. 6(a) and (b) respectively, establishing pore

Table 2
Ratios of RCP values and $(\phi\beta)^*$ of modified and plain concretes.

Mixture ID	28 days					90 days				
	$RCP_{plain} \div RCP_{modified}$ (x)	$(\phi\beta)^*$		$(\phi\beta)^*/x$		$RCP_{plain} \div RCP_{modified}$ (x)	$(\phi\beta)^*$		$(\phi\beta)^*/x$	
		Before	After	Before	After		Before	After	Before	After
Plain	1.00	1.00	1.00	1.00	1.00	1.00	1.00	1.00	1.00	1.00
FA10	1.07	1.00	0.92	0.93	0.86	1.18	1.12	1.03	0.95	0.87
FA20	1.03	1.01	1.01	0.98	0.98	1.77	1.60	1.28	0.90	0.72
SF6	2.45	1.85	1.70	0.75	0.69	2.55	1.76	1.40	0.69	0.55
SF9	3.78	2.65	2.55	0.70	0.67	4.99	3.30	3.08	0.66	0.62

$(\phi\beta)^* = (\phi\beta)_{plain\text{-}concrete}/(\phi\beta)_{modified\text{-}concrete}$.

connectivity as an important pore structure feature that can be related to both these rapid chloride transport parameters.

Though it is known that reduction in porosity and pore connectivity is critical to achieving reduced chloride transport, it is instructive to examine the relationship between β and ϕ for mixtures that are compositionally different. A cursory look at Eq. (6) shows that the pore volume fraction and the pore geometry (or connectivity) are expressed as separate terms, and thus might lead to the observation that they are inherently independent. But it needs to be remembered that the reduction in both the overall pore volume and the connectivity of the pore network in cement pastes or concretes is a consequence of the hydration of the cement (and cement replacement materials, if any). Therefore, even when the mathematical expression shows inherent independence, β and ϕ can be considered as related through the hydration process of the cementing materials.

Fig. 7 shows the relationship between porosity and pore connectivity factor for all the mixtures used in this study, at all ages. In general, a reduction in porosity results in a reduction in pore connectivity. Two different trends are immediately discernible — one with a flatter slope for plain and fly ash modified mixtures, and one with a steeper slope for the silica fume modified mixtures. The plot area is divided into a 3×3 square grid, with porosity increments of 1.1%, and pore connectivity increments of 0.006. The grid A-1 corresponds to the lowest values of ϕ and β (very high pore structure refinement), and grid C-3 corresponds to the highest values of ϕ and β (low or negligible pore refinement). Moving horizontally from right to left in the plot area indicates reduction in porosity, and moving vertically from top to bottom indicates reduction in pore connectivity. The plain concrete mixture lies in the grid C-2 at early ages and in grid B-2 at later ages, demonstrating a lower degree of pore refinement. The fly ash modified mixtures at early age lie in grid C-3 where as at later ages they are placed in grid B-1, indicating significant reductions in both ϕ and β. The silica fume modified mixtures move from grid B-2 to A-2 with increase in age and silica fume content. There is a large reduction in β for these mixtures. When the values of the transport parameters as shown in the table below Fig. 7 are observed, significant reductions in the values of RCP and D_{nssm} are seen when moving along the C–B–A path rather than the 3–2–1 path in the plot. In other words, a reduction in pore connectivity is found to be much more efficient in reducing chloride transport than porosity reduction.

Table 3
Porosities of the plain and modified concretes.

Mixture ID	Porosity (%)		
	28 days	56 days	90 days
Plain	7.20	6.75	6.37
FA10	7.84	6.91	5.99
FA20	7.55	6.50	5.20
SF6	7.10	6.79	6.33
SF9	6.95	6.62	6.14

5.2. Equivalent electrical circuit model parameters for concrete microstructure

The discussions in the previous section have focused on the inter-relationship between the two microstructural features (porosity and pore connectivity) extracted from the experimentally measured conductivities, as well as their relationship with the chloride transport parameters. In this section, an equivalent circuit model is used for the electrical impedance spectra of concretes before they were subjected to chloride transport with an aim to relate the characteristic features of this model to the chloride transport parameters.

5.2.1. Equivalent circuit model for EIS spectra of concretes

Various equivalent electrical circuit models have been presented in the literature to model the electrical impedance spectra of concretes [37–39]. These models invariably consist of combinations of resistors, capacitors, and constant-phase elements. As mentioned earlier, EIS studies were conducted on concretes placed in the RCPT cells with the anolyte and catholyte in place. A circuit model that has been shown to represent the bulk arc in the impedance spectra fairly accurately [21,23] is used, which is shown in Fig. 8(a). In the model, R_e corresponds to the resistance of the electrolyte in between the specimen and the electrode, R_c is the resistance attributed to the ionic motion in pores that are connected from one end of the sample to the other (or percolating pores), R_{uc} is the resistance attributed to the ionic motion in the unconnected pores, and R_i is the resistance associated with the electrolyte–concrete interface. The capacitances C_s, C_p, and C_i are associated with the solid fraction in the specimen, the pore walls, and the electrolyte–concrete interface respectively.

The overall frequency-dependent impedance of the model, $Z(\omega)$, is given as:

$$Z(\omega) = R_e + \frac{Z_1 Z_2}{Z_1 + Z_2} + Z_3. \quad (9)$$

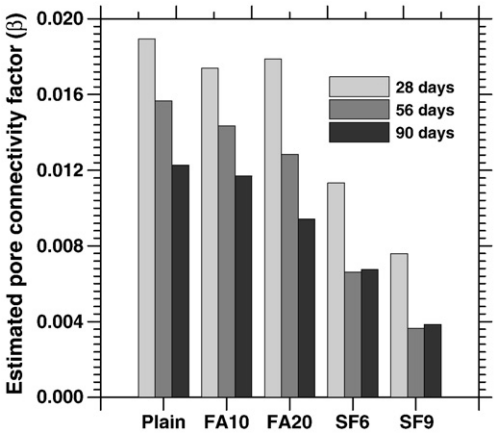

Fig. 5. Pore connectivity factors for the plain and modified concrete mixtures.

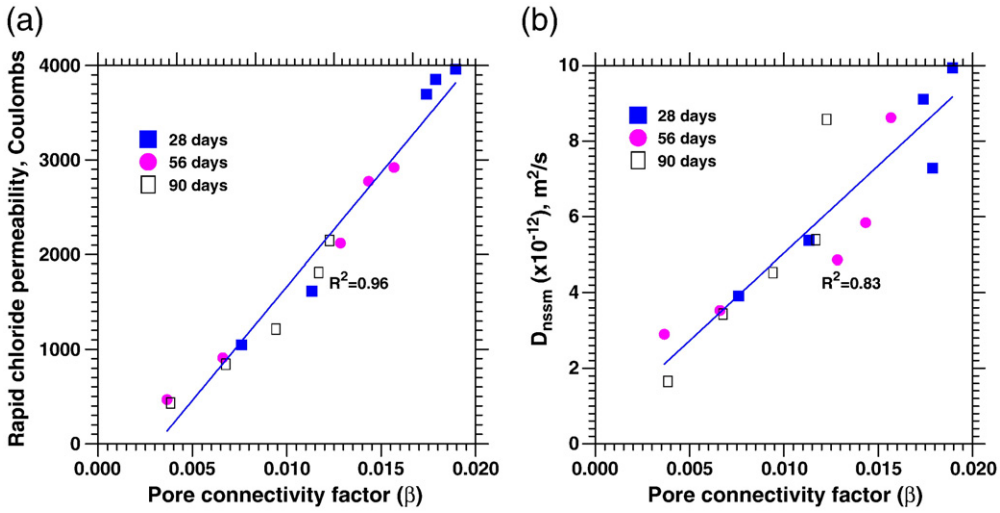

Fig. 6. Pore connectivity factor and its relationship to: (a) rapid chloride permeability, and (b) non-steady state migration values.

Z_1, Z_2, and Z_3 are the impedances of the element groups in the circuit. Z_1 and Z_2 correspond to the bulk of the specimen. The impedances Z_1 and Z_2 are in parallel as shown in Fig. 8(a), with Z_1 representing the impedance of the combination of R_c and C_s, and Z_2 representing the impedance of the combination of R_{uc} and C_p. Z_1 and Z_2 are given as:

$$Z_1 = \frac{R_c}{1 + (j\omega R_c C_s)^{\alpha}} \tag{10a}$$

$$Z_2 = R_{uc}\left[1 + \left(j\omega R_{uc} C_p\right)^{-\beta}\right]. \tag{10b}$$

The terms α and β are the dispersion factors. The equivalent circuit model parameters were extracted from the impedance spectra using ZView™ software. Fig. 8(b) shows representative experimental impedance spectra (symbols) and the bulk arc fitted using the model described by Eq. (9) (solid lines).

Percolating pores in concrete dominate the transport properties. Hence, in this paper, the resistance of the connected pores (R_c) obtained from the equivalent circuit model is considered to be an important parameter that can be related to the chloride transport, and further discussions are limited to R_c. Fig. 9(a) and (b) shows the variation in RCP and D_{nssm} values with the resistance of connected pores (R_c) obtained from the equivalent circuit model. With increasing values of R_c, both the RCP as well as D_{nssm} values are found to decrease, as expected. However, a pattern emerges from both these figures — the reduction in RCP and D_{nssm} values is rapid for R_c values up to about 750 Ω, denoted by the vertical lines in these figures. Beyond that, the drop in RCP and D_{nssm} values is very gradual and minimal even though the R_c values increase significantly. In both these figures, the points lying in the zone of gradual decline of the transport parameters (to the right of the vertical line) correspond to silica fume modified concretes at 56 and 90 days of curing. When the pore connectivity factor (β) values are plotted against the R_c values as shown in Fig. 9(c), a trend similar to those in Fig. 9(a) and (b) is observed, indicating that the change in β for the specimens to

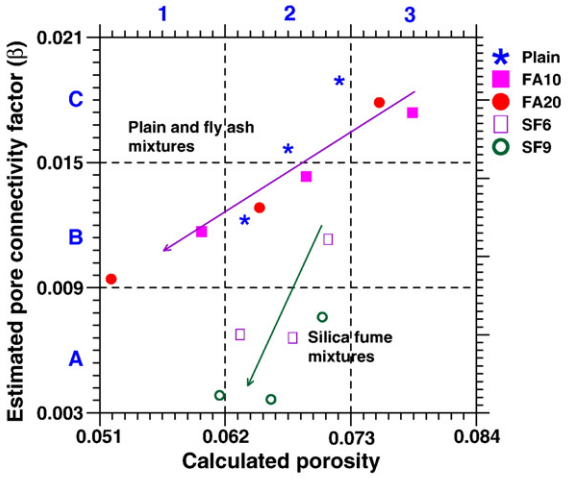

φ → / β ↓	1		2		3	
	RCP (Coulombs)	D_{nssm} x 10^{-12} (m^2/s)	RCP (Coulombs)	D_{nssm} x 10^{-12} (m^2/s)	RCP (Coulombs)	D_{nssm} x 10^{-12} (m^2/s)
A			400-900	1.60-4.0		
B	1200-1800	4.50-5.40	1600-2800	4.80-8.50		
C			2900-4000	8.60-10.0	3600-4000	7.0-9.0

Fig. 7. Porosity–pore connectivity relationships for the modified concretes and their influence on transport parameters.

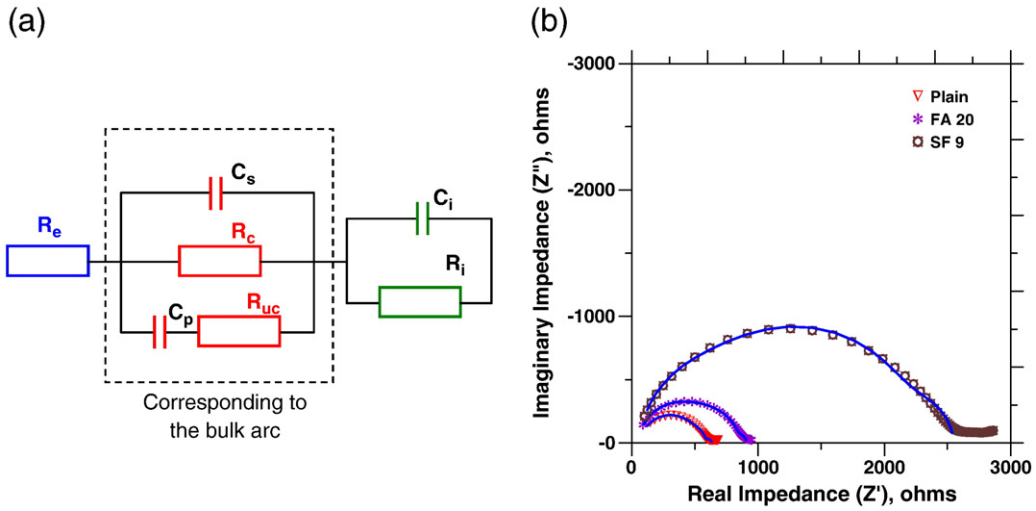

Fig. 8. (a) Equivalent electrical circuit model for the concretes, and (b) representative fits of the bulk arc of the Nyquist plots using the model.

the right of the vertical line at 750 Ω in Fig. 9(a) and (b) is not very high. The similarity of Fig. 9(c) to (a) and (b) again shows that the transport parameters are very much dependent on the pore connectivity, which is adequately captured by the modeled resistance of the connected pores. The large increase in R_c observed for the silica fume modified mixtures without a drastic reduction in pore connectivity could be attributed to a reduction in the sizes of the pores. Since resistance is inversely proportional to the square of the pore size, even a moderate reduction in the size will result in a large increase in the resistance, as observed in these figures. Quantification of the pore size reduction accomplished by the incorporation of silica fume or fly ash is provided in the following section using an idealized equivalent pore model.

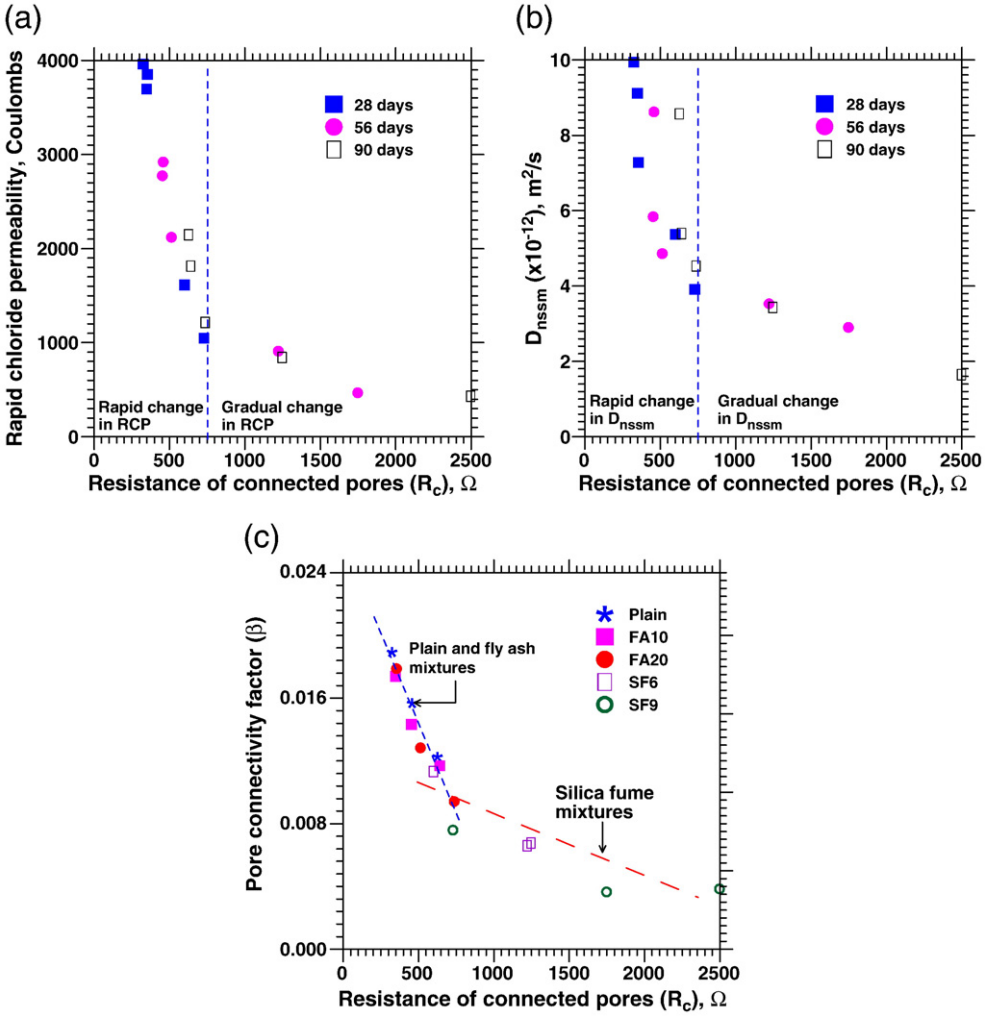

Fig. 9. Relationship between the resistance of connected pores and: (a) RCP values, (b) non-steady state migration values, and (c) pore connectivity.

In Fig. 9(c), the relationship between pore connectivity and R_c is plotted using different symbols for all the five different mixtures (instead of different symbols for three different ages as shown in the other two figures) in order to bring out the point that plain and fly ash modified mixtures behave similarly, and they differ considerably from the silica fume modified mixtures as far as the R_c values are concerned. This might be construed as an indication of the similarities in the pore structure between plain and fly ash concretes, and their considerable differences with the pore structure of silica fume modified concretes, which is the subject of the following analysis.

5.2.2. Equivalent pore sizes and pore size reduction efficiency derived from R_c

R_c as described in the previous section is effectively the resistance attributable to all the connected pores in the system filled with the pore solution. If the connected pore system in the material can be idealized into one single pore that retains the entire features of the combined pore system, R_c can be expressed as:

$$R_c = \frac{L_{conn}}{\sigma_{conn} A_{conn}}. \quad (11)$$

L_{conn} is the length, σ_{conn} is the conductivity, and A_{conn} is the area respectively of the idealized connected pore. Since the only conducting element in a pore is the pore solution, σ_{conn} can be taken to be approximately equal to the pore solution conductivity, σ_{pore}. This is strictly not correct because the conductivity of the pore will also depend on its geometry, and will likely be lower than the conductivity of the solution that fills it. If τ is the tortuosity of the idealized connected pore, then $L_{conn} = L\tau$, where L is the length of the sample (50 mm in the case of RCP and NSSM test specimens). The tortuosity can be expressed as a function of the porosity and formation factor (ratio of pore solution conductivity to effective conductivity of the sample) as [40]:

$$\tau^2 = \frac{\sigma_{pore}}{\sigma_{eff}}\phi. \quad (12)$$

Combining Eq. (6) for effective conductivity, and Eq. (12), it follows that the tortuosity (τ) and the pore connectivity factor (β) are related as:

$$\tau = \beta^{-1/2}. \quad (13)$$

Substituting these values in Eq. (11), and simplifying gives the equivalent diameter of the idealized connected pore (d_{conn}) as:

$$(d)_{conn} = 2\sqrt{\frac{L\beta^{-1/2}}{\pi R_c \sigma_{pore}}}. \quad (14)$$

The values of σ_{pore} and β can be obtained from Figs. 4 and 5 respectively. The equivalent pore diameters predicted using Eq. (14) for all the mixtures at different ages are shown in Fig. 10. It must be noted that large values of equivalent pore diameters (in the range of 6 mm–11 mm) are obtained from the model because it is assumed in the model formulation that all connected pores in the material under consideration are idealized into one single pore. The trends in this figure show that the pore sizes in plain and fly ash modified concretes are similar, especially at early ages, but they are considerably different from those of the silica fume modified concretes which are much lower. At later ages, though the effect of pore size refinement is evident in fly ash modified concretes, it is not as significant as compared to silica fume modified concretes.

Fig. 11(a) shows the relationship between the idealized pore diameters derived from the model using R_c and the pore connectivity factor (β) for all the mixtures. The pore connectivity factors are found to decrease with decreasing pore sizes. Two separate relationships could be identified from this figure — one for the plain and fly ash modified mixtures, and the other for silica fume modified mixtures. The silica fume modified mixtures show lower pore connectivity factors for the same pore size, and the higher the silica fume content in the mixture, the lower the pore connectivity. Fig. 11(b) is the representation of the porosity of all the concretes when plotted against the idealized pore diameters. Both these figures facilitate a comparative model-based evaluation of how porosity and pore connectivity are related to the pore sizes. While a reduction in either porosity or the equivalent pore diameter indicates a general reduction in the other, two separate relationships are observed in this figure too — one for the plain and fly ash concretes, and the other for silica fume modified concretes. Smaller pore sizes seem to suggest lower porosities for the plain and fly ash modified concretes, whereas the porosity reductions for the silica fume modified concretes are not as pronounced, as was observed from the experimental results earlier in this paper as well as other studies [34,41]. Fig. 11(a) shows that pore size reduction is vital to pore connectivity reduction while Fig. 11(b) does not present a compelling evidence of porosity reduction in silica fume modified concretes with reducing pore sizes. However, the chloride transport parameters are found to be consistently lower for the silica fume modified concretes. This leads to the conclusion that although porosity reduction does play a role in reducing pore connectivity as seen from Fig. 7, it is the lower pore sizes that contribute significantly to lowering the pore connectivity, and thus towards beneficial transport properties.

6. Conclusions

This study has provided relationships between the rapid chloride transport parameters of concretes modified with fly ash or silica fume and some of the important microstructural parameters derived using electrical impedance based methods on these concretes either directly or through the use of models. The following conclusions are arrived at based on this study.

(i) The modified concretes were found to exhibit lower RCP and NSSM coefficients (D_{nssm}), with the silica fume modified concretes showing the lowest values, as expected. The RCP values were found to be very well related to the initial conductivity values obtained from electrical impedance whereas the D_{nssm} values had a slightly weaker relationship with initial conductivity, possibly because of the microstructural changes occurring in the specimen while being subjected to the longer duration of the NSSM test. The D_{nssm} values were found to be much higher than the steady state diffusivities (D_{SSC}).

(ii) A methodology was detailed in this paper that quantifies the influence of pore solution conductivity and pore structure refinement on the RCP values of modified concretes, relative to

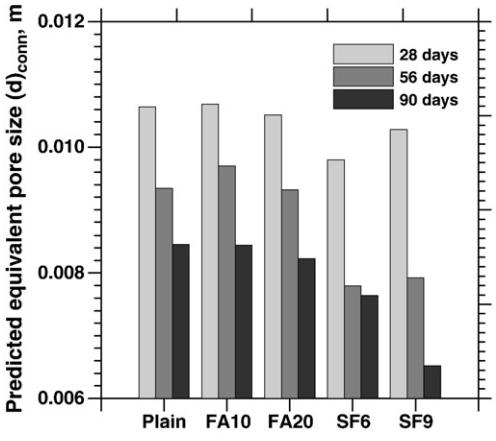

Fig. 10. (a) Predicted idealized equivalent pore diameters from the circuit model.

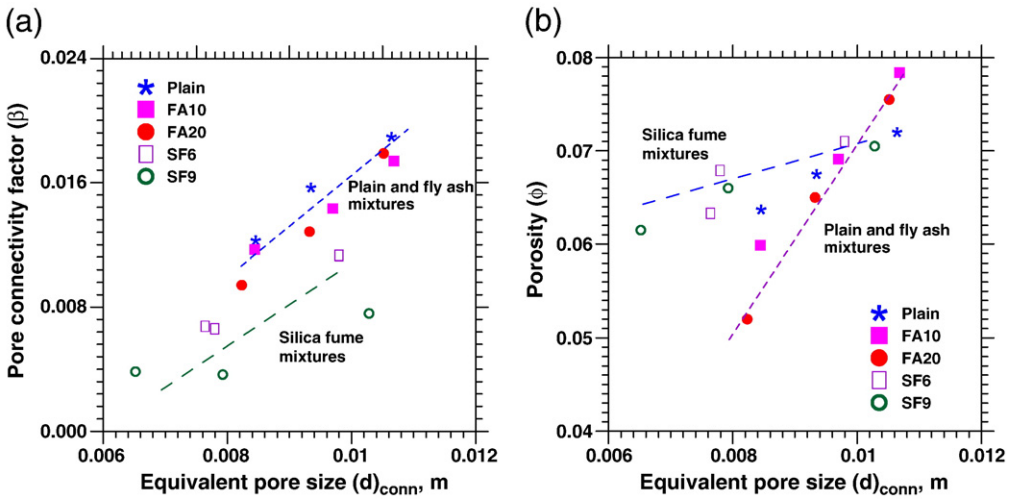

Fig. 11. (a) Relationships between equivalent pore size and: (a) pore connectivity, and (b) porosity of concretes.

that of plain concrete. This method utilized the ratio of the RCP values of the plain and modified concretes, as well as the ratios of effective conductivities and pore solution conductivities of plain and modified concretes. For the silica fume modified concretes used in this study, for various ages, this method predicted that 66–75% of the reduction in RCP values with respect to plain concrete can be attributed to pore structure refinement while the corresponding value was more than 90% for fly ash modified mixtures. This is consistent with the understanding that a reduction in pore solution conductivity is partly responsible for lower RCP values of silica fume modified concretes.

(iii) The pore connectivity factor was found to be linearly related to both RCP and D_{nssm} values, establishing pore connectivity as an important microstructural feature in dictating chloride transport. When the porosity–pore connectivity relationships were explored, it was observed that in general, a reduction in porosity resulted in a reduction in pore connectivity. When the changes in rapid chloride transport parameters were compared to the changes in porosity and pore connectivity, it was seen that a reduction in pore connectivity impacts the transport parameters much more than a reduction in porosity.

(iv) An electrical circuit model was used along with the impedance spectra of concretes in order to extract pertinent features of the microstructure that can be related to transport properties. Since the percolating pores are most influential in transport, the resistance of the connected pores (R_c) was used as the electrical property that characterizes the pore structure. The relationship of R_c with RCP, D_{nssm}, and the pore connectivity (β) values were found to be similar. For the plain and fly ash modified mixtures, the increase in R_c that resulted in a reduction of RCP, D_{nssm} or β was lower as compared to the increase in R_c for silica fume modified mixtures.

(v) The values of R_c obtained from the circuit model were used to determine the equivalent size of an idealized connected pore that retains all the features of the pore system in the concrete. Reduced pore sizes were invariably found to result in lower pore connectivities but the same could not be stated about the porosity, especially for silica fume modified concretes. Since silica fume modified concretes showed reduced chloride transport parameters, this lead to the conclusion that pore size reduction contributed more significantly than porosity reduction towards reducing the pore connectivity, which ultimately results in beneficial transport properties.

References

[1] H.-W. Song, C.-H. Lee, K.Y. Ann, Factors influencing chloride transport in concrete structures exposed to marine environments, Cement Concr. Compos. 30 (2008) 113–121.
[2] G.K. Glass, N.R. Buenfeld, Chloride-induced corrosion of steel in concrete, Prog. Struct. Eng. Mater. 2 (2000) 448–458.
[3] M. Hisada, S. Nagataki, N. Otsuki, Evaluation of mineral admixtures on the viewpoint of chloride ion migration through mortar, Cement Concr. Compos. 21 (1999) 443–448.
[4] K.A. Gruber, T. Ramlochan, A. Boddy, R.D. Hooton, M.D.A. Thomas, Increasing concrete durability with high reactivity metakaolin, Cement Concr. Compos. 23 (2001) 479–484.
[5] M.S. Ahmed, O. Kayali, W. Anderson, Chloride penetration in binary and ternary blended cement concretes as measured by two rapid methods, Cement Concr. Compos. 30 (2008) 576–582.
[6] L. Tang, L.-O. Nilsson, Chloride binding capacity and binding isotherms of OPC pastes and mortars, Cement Concr. Res. 23 (1993) 247–253.
[7] H. Zibara, R.D. Hooton, M.D.A. Thomas, K. Stanish, Influence of the C/S and C/A ratios of hydration products on the chloride ion binding capacity of lime-SF and lime-MK mixtures, Cement Concr. Res. 38 (2008) 422–426.
[8] Q. Yuan, C. Shi, G. De Schutter, K. Audenaert, D. Deng, Chloride binding of cement based materials subjected to external chloride environment — a review, Constr. Build. Mater. 23 (2009) 1–13.
[9] R.F. Feldman, G.W. Chan, R.J. Brousseau, P.J. Tumidajski, Investigation of the rapid chloride permeability test, ACI Mat. J. 91 (1994) 246–255.
[10] K.D. Stanish, R.D. Hooton, M.D.A. Thomas, Testing the Chloride Penetration Resistance of Concrete: A Literature Review, FHWA Contract DTFH61-97-R-00022, University of Toronto, Toronto, Ontario, Canada, June 2000.
[11] T. Gardner, K. Stanish, M. Alexander, Critical review of rapid chloride test methods for concrete, Concr. Beton 113 (2006) 11–17.
[12] NT BUILD 492, Concrete, Mortar and Cement-based Repair Materials: Chloride Migration Coefficient from Non-steady-state Migration Experiments, Nordtest Method, 492, 1999.
[13] P.E. Streicher, M.G. Alexander, A chloride conduction test for concrete, Cement Concr. Res 25 (1995) 1284–1294.
[14] L. Tang, Concentration dependence of diffusion and migration of chloride ions. Part 1: theoretical considerations, Cement Concr. Res 29 (1999) 1463–1468.
[15] G.A. Narsilio, R. Li, P. Pivonka, D.W. Smith, Comparative study of methods used to estimate ionic diffusion coefficients using migration tests, Cement Concr. Res 37 (2007) 1152–1163.
[16] C.T. Chiang, C.C. Yang, Relation between the diffusion characteristic of concrete from salt ponding test and accelerated chloride migration test, Materials Chemistry and Physics 106 (2007) 240–246.
[17] B.J. Christensen, R.T. Coverdale, R.A. Olson, S.J. Ford, E.J. Garboczi, H.M. Jennings, T.O. Mason, Impedance spectroscopy of hydrating cement-based materials: measurement, interpretation and application, J. Am. Ceram. Soc. 77 (1994) 2789–2804.
[18] W.J. McCarter, T.M. Chrisp, G. Starrs, J. Blewett, Characterization and monitoring of cement based systems using intrinsic electrical property measurements, Cement Concr. Res. 33 (2003) 197–206.
[19] G.M. Moss, B.J. Christensen, T.O. Mason, H.M. Jennings, Microstructural analysis of young cement pastes using impedance spectroscopy during pore solution exchange, Advanced Cement Based Materials 4 (1996) 68–75.
[20] M. Shi, Z. Chen, J. Sun, Determination of chloride diffusivity in concrete by AC impedance spectroscopy, Cement Concr. Res. 29 (1999) 1111–1115.

[21] B. Diaz, X.R. Nóvoa, M.C. Pérez, Study of the chloride diffusion in mortar: a new method of determining diffusion coefficients based on impedance measurements, Cement Concr. Compos. 28 (2006) 237–245.
[22] J.M. Loche, A. Ammar, P. Dumargue, Influence of the migration of chloride ions on the electrochemical impedance spectroscopy of concrete paste, Cement Concr. Res. 35 (2005) 1797–1803.
[23] I. Sánchez, X.R. Nóvoa, G. de Vera, M.A. Climent, Microstructural modifications in portland cement concrete due to forced ionic migration tests: study by impedance spectroscopy, Cement Concr. Res. 38 (2008) 1015–1025.
[24] K.A. Synder, C. Ferraris, N.S. Martys, E.J. Garboczi, Using impedance spectroscopy to assess the viability of rapid chloride test for determining chloride conductivity, Journal of Research of National Institute of Standards and Technology 105 (4) (2000) 497–509.
[25] RILEM CPC 11.3, Absorption of water by immersion under vacuum, Mater. Struct. 17 (1984) 391–394.
[26] K. Torii, M. Kawamura, Pore structure and chloride ion permeability of mortars containing silica fume, Cement Concr. Compos. 16 (1994) 279–286.
[27] G.A. J-Betancourt, R.D. Hooton, Study of the Joule effect on rapid chloride permeability values and evaluation of related electrical properties of concretes, Cement Concr. Res. 43 (2004) 1007–1015.
[28] J. Jain, N. Neithalath, accepted for publication. Chloride transport in fly ash and glass powder modified concretes — influence of test methods on microstructure, Cement and Concrete Composites 32 (2010) 148–156.
[29] R. Mills, The self-diffusion of chloride ions in aqueous alkali chloride solutions at 25°, Journal of Physical Chemistry 61 (12) (1957) 1631–1634.
[30] L. Tong, O.E. Gjørv, Chloride diffusivity based on migration testing, Cement Concr. Res. 31 (2001) 973–982.
[31] K.A. Snyder, X. Feng, B.D. Keen, T.O. Mason, Estimating the conductivity of cement paste pore solutions from OH^-, K^+ and Na^+ concentrations, Cement Concr. Res. 33 (2003) 793–798.
[32] H.F.W. Taylor, A method for predicting alkali ion concentrations in cement pore solutions, Adv. Cem. Res. 1 (1987) 5–17.
[33] N. Schwarz, N. Neithalath, Influence of a fine glass powder on cement hydration: comparison to fly ash and modeling the degree of hydration, Cement Concr. Res. 38 (2008) 486–496.
[34] N. Neithalath, J. Persun, A. Hossain, Hydration in high-performance cementitious systems containing vitreous calcium aluminosilicate or silica fume, Cement Concr. Res. 39 (2009) 473–481.
[35] G. Sant, D.P. Bentz, J. Weiss, 2010. Examining capillary depercolation in cement-based materials: measurement techniques and parameters which influence their interpretation, personal communication.
[36] D.P. Bentz, A virtual rapid chloride permeability test, Cement Concr. Compos. 29 (2007) 723–731.
[37] G. Song, Equivalent circuit model for AC electrochemical impedance spectroscopy of concrete, Cement Concr. Res. 30 (2000) 1723–1730.
[38] M. Cabeza, M. Keddam, X.R. Nóvoa, I. Sánchez, H. Takenouti, Impedance spectroscopy to characterize the pore structure during the hardening process of Portland cement paste, Electrochim. Acta 51 (2006) 1831–1841.
[39] D.E. Macphee, D.C. Sinclair, S.L. Cormack, Development of an equivalent circuit model for cement pastes from microstructural considerations, J. Am. Ceram. Soc. 80 (1997) 2876–2884.
[40] D.C. Herrick, W.D. Kennedy, Electrical efficiency — a pore geometric theory for interpreting the electrical properties of reservoir rocks, Geophysics 59 (1994) 918–927.
[41] J. Yajun, J.H. Cahyadi, Effects of densified silica fume on microstructure and compressive strength of blended cement pastes, Cement Concr. Res. 33 (2003) 1543–1548.